International Journal of Nanomedicine

Dovepress
open access to scientific and medical research

Open Access Full Text Article

ORIGINAL RESEARCH

On the Ion Implantation Synthesis of Ag-Embedded Over Sr-Substituted Hydroxyapatite on a Nano-Topography Patterned Ti for Application in Acetabular Fracture Sites

Subhasmita Swain[1], Monalisa Pradhan[1,*], Samapika Bhuyan[1,*], RDK Misra[2], Tapash R Rautray[1]

[1]Biomaterials and Tissue Regeneration Laboratory, Centre of Excellence, Siksha 'O' Anusandhan (Deemed to Be University), Bhubaneswar, Odisha, 751030, India; [2]Metallurgical, Materials and Biomedical Engineering Department, the University of Texas at El Paso, El Paso, TX, 79968, USA

*These authors contributed equally to this work

Correspondence: Tapash R Rautray, Tel +91 9040000604, Email tapashrautray@soa.ac.in

Introduction: There is an ongoing need for improved healing response and expedited osseointegration on the Ti implants in acetabular fracture sites. To achieve adequate bonding and mechanical stability between the implant surface and the acetabular fracture, a new coating technology must be developed to promote bone integration and prevent bacterial growth.

Methods: A cylindrical Ti substrate mounted on a rotating specimen holder was used to implant Ca^{2+}, P^{2+}, and Sr^{2+} ions at energies of 100 KeV, 75 KeV and 180 KeV, respectively, using a low-energy accelerator to synthesize strontium-substituted hydroxyapatite at varying conditions. Ag^{2+} ions of energy 100 KeV were subsequently implanted on the as-formed surface at the near-surface region to provide anti-bacterial properties to the as-formed specimen.

Results: The properties of the as-formed ion-implanted specimen were compared with the SrHA-Ag synthesized specimens by cathodic deposition and low-temperature high-speed collision technique. The adhesion strength of the ion-implanted specimen was 43 ± 2.3 MPa, which is well above the ASTM standard for Ca-P coating on Ti. Live/dead cell analysis showed higher osteoblast activity on the ion-implanted specimen than the other two. Ag in the SrHA implanted Ti by ion implantation process showed superior antibacterial activity.

Discussion: In the ion implantation technique, nano-topography patterned surfaces are not concealed after implantation, and their efficacy in interacting with the osteoblasts is retained. Although all three studies examined the antibacterial effects of Ag^{2+} ions and the ability to promote bone tissue formation by MC3T3-E1 cells on SrHA-Ag/Ti surfaces, ion implantation techniques demonstrated superior ability. The synthesized specimen can be used as an effective implant in acetabular fracture sites based on their mechanical and biological properties.

Keywords: titanium, SrHA-Ag, ion implantation, osteogenic, anti-bacterial

Introduction

Acetabular fracture is a frequently occurring disease in the field of orthopaedics. Pathological acetabular fractures, produced by osteoporotic bone, result from insufficient mechanical stress. The prevalence of these fractures among the elderly has lately shown a significant rise, mainly attributed to the combination of increased overall mortality and a relative decline in trauma cases among younger persons.[1] The chances of a positive clinical result are reduced in elderly people due to impaired physiologic reserve and reduced healing ability treatments. The advancement of bone substitutes, innovative imaging techniques, and fixation treatments might improve the future treatment of acetabular fractures.[2] According to the literature, the need for orthopaedic implants among patients has grown substantially in the last few years. Therefore, it is imperative that patients with orthopaedic disorders be treated and their quality of life as a whole be

Received: 20 February 2024
Accepted: 15 May 2024
Published: 21 May 2024

increased, depending on the development of an implant device.[3] Subsequently, metallic biomaterials, such as titanium (Ti) and its alloys, are highly advantageous for fixing bone fractures and joint prostheses for their outstanding biocompatibility, increased tensile strength, enhanced corrosion resistance, wear resistance, and low allergy risk, and they have been extensively used as biomedical implant material.[4,5] Consequently, there is a persistent demand for enhanced healing response and accelerated bone growth in the context of acetabular fractures.[6] To attain significant osseointegration between the implant surface and the bone, it is necessary to modify the surface of the implants.[7] The application of an etching solution to the Ti-based material may result in the formation of an intricate and consistent arrangement of nano-sized pits on the surface, which can drastically improve the osteogenicity of the implant.[8] The modified surface exhibits a notable resistance to corrosion, the capacity to adsorb proteins, the ability to stimulate the growth of bone cells, and ultimately ensures osseointegration between bone-to-implant contact. Additionally, it inhibits the formation of fibrous tissues to enhance osteoblast activity.[9]

Various techniques, such as plasma spray, electrochemical, sol-gel, sputtering, biomimetic, laser cladding, etc., are used to develop coatings on implant surfaces.[10–12] However, these techniques have certain limitations in various aspects. Therefore, there is a need to develop a novel coating that possesses exceptional capability to enhance osteogenicity and suppress bacterial activity without any adverse effects. Although plasma spray is a state-of-The-art technique, it generates thick coatings with various phases exhibiting mixed crystallinity and different dissolution rates of the coating composition.[13]

Furthermore, a bacterial infection might impact implant failure because a developed bacterial biofilm on the implant surface may render antibiotics ineffective. Hence, it is essential to develop surfaces that prevent the attachment of bacteria and enable the gradual release of antimicrobial agents that can effectively disrupt bacterial biofilms. To prioritize the development of such surfaces is essential to ensure the safety and effectiveness of implants.[14]

Consequently, the observed antibacterial properties of silver (Ag) have resulted in its widespread application in healthcare. Ag nanoparticles (AgNPs) are increasingly used in orthopaedic implants and treat implant-associated infections because of their ability to penetrate and destroy bacterial cells rapidly. It has been found from the literature that AgNPs can effectively prevent bacterial cells from further multiplying.[15] Moreover, a study conducted by Zhang et al has shown that the incorporation of Sr and Ag to the titanium dioxide (TiO_2) coating has significant osteogenic and antibacterial properties.[16] As stated earlier, HA is an essential component in promoting osseointegration at the interface of the bone and implant. However, the deposition of hydroxyapatite [$Ca_{10}(PO_4)_6(OH)_2$, HA] onto titanium implant substrates via ion implantation has been suggested as a prospective strategy to enhance surface bioactivity and osteogenicity. As compared to plasma-sprayed HA coating, which may lead to issues such as the release of coating debris, infiltration of macrophages, encapsulation by fibrous tissues and possible implant failure,[17] the apatite surface created by ion implantation can significantly enhance the early formation of bone into porous surfaces. This technique allows for precise control over the ion concentration, distribution, and depth of calcium and phosphorus deposited on the surface, resulting in a significant increase in adhesion strength.[18,19] The utilization of metal-incorporated calcium-phosphate (Ca-P) ceramics in biomedical applications, particularly in the field of bone regeneration, has generated significant interest.[20] So, the synthesis of HA by ion implantation provides outstanding mechanical properties simultaneously exhibiting higher osteogenicity. While conventional ceramic coatings are unsuitable for load-bearing applications or for application in extensive bone defects because of their weak mechanical properties, HA nanoparticles formed by ion implantation can overcome these drawbacks.[21,22]

Strontium (Sr) has undergone extensive research and is well recognized for its osteogenic properties, whereas the amount of Sr substituted in the Ca site of HA impacts the shape, structure of apatite, and crystallinity of Ca-P ceramics.[23,24] These characteristics, in turn, affect the solubility of the coating, the in vitro behaviour of osteoblasts and osteoclasts and the in vivo bone remodelling processes. Due to ongoing dissolution and precipitation, the SrHA surface exhibits reactivity and biodegradability, forming apatite resembling osseous tissue on its surface. SrHA stimulates the formation of new bone by bone marrow stem cells (BMSCs), minimizes the time required for bone healing, and improves the integration of implants with the surrounding bone tissue.[25]

The present investigation focuses on the synthesis of Sr substituted HA on a rotating cpTi implant using Ca^{2+}, P^{2+} and Sr^{2+} ions produced from a low energy ion beam linear accelerator and subsequently, Ag^{2+} was flash coated (low-dose implantation) after the formation of SrHA onto the nano-topography patterned cpTi surface. Furthermore, various

analytical techniques were employed to assess the mechanical and biological properties of the specimens. The specimens were also modified using two different surface modification techniques, such as cathodic deposition (CD) and Low Temperature High Speed Collison (LTHSC) methods, and their properties were compared. Hence, this study provides invaluable insights into the surface structure design of biomedical implants that promote successful osteogenesis, making it an essential contribution to the biomedical fields.

Materials and Methods

Pretreatment of Ti Sheet

Commercially pure titanium (cpTi, grade 4) surface was polished in a single direction longitudinally to form nano patterns using 600–1200 SiC grit papers. cpTi substrates were etched in a mixture of 1 part HF, 4 parts HNO_3 and 5 parts water. Nano-topographical cpTi surfaces were further processed by boiling in a 10 M NaH_2 solution at 60°C for 24 h. Then, the substrates were washed with deionized water and dried overnight in a dark atmosphere at room temperature. The cpTi specimens were then sintered at 600°C at a linearly increasing temperature of 5°C/min for 1h to obtain the nano-topographical surface on Ti. Then, the substrate underwent ultrasonic cleaning using deionized water, acetone, and toluene. After drying in air, the Ti substrates were kept in a desiccator until they were coated with Ag-SrHA by ion implantation, CD and LTHSC techniques.[26]

Fabrication of Rotating Specimen Holder for Ion Implantation Technique

The Ti substrate was rolled into a cylindrical shape and mounted on a rotating specimen holder driven by an electric motor. The idea behind the use of a cylindrical sample holder is to (i) synthesize multiple specimens in a single loading (cut into pieces after implantation), (ii) reduce specimen loading time- and (iii) enhance the line-of-sight area under 3D rotation of the specimen. Subsequently, Ca^{2+}, P^{2+}, and Sr^{2+} ions at different energies were implanted on its surface. Before cell culture, both the control and ion-implanted Ti were sterilized using ultraviolet radiation and kept in a desiccator at room temperature.

Ag Flash-Coated Sr-HA Deposition on Ti Surface by Ion Implantation (SrHA-Ag/Ti (Ion-Implanted))

Using a low-energy linear accelerator (50 keV Ion implanter, Source: Multi-cathode source of negative ions by cesium sputtering ion source), implantation of Ca^{2+}, P^{2+} and Sr^{2+} ions was carried out. CaO was used as the source cathode material for the Ca^{2+} ions, while GaP was utilised as the source cathode material for the PO_4^{3-} ions and SrH_2 was used as the source cathode material for obtaining Sr^{2+} ions. A rotating cylindrical cpTi (purity 99.2%), with dimensions of Φ 9.6 mm × height 15 mm affixed on the sample holder was implanted with ^{40}Ca, ^{31}P, and ^{88}Sr beams. A uniformly implanted area of 10 × 30 mm^2 was taken as the active implantation area. To synthesize SrHA, ion energies of 100 KeV for Ca^{2+} and, 75 KeV for P^{2+}, 180 KeV for Sr^{2+} were used with a beam current density of 100 nA/cm^2, 200 nA/cm^2 and 230 nA/cm^2 for Ca^{2+}, P^{2+} and Sr^{2+}, respectively. The purpose of choosing different ion energies was to implant the ions (Ca^{2+}, P^{2+} and Sr^{2+}) at the same implantation depth so that subsequent physical conditions would bring them together to interact. The vacuum of the implantation chamber was kept at 4×10^{-5} Pa during P^{2+} implantation. The Ca^{2+} implantation was carried out by backfilling oxygen at a pressure of 1.7×10^{-3} Pa in the implantation chamber to obtain CaO on the Ti surface. At the end of Ca^{2+} ion implantation, the maximum concentration of Ca^{2+} and the dose of Ca^{2+} (which is the number of implanted Ca^{2+} atoms/cm^2) was enhanced in the Ti substrate with a fluence of 2×10^{16} Ca^{2+} ions/cm^2. In contrast, the fluence for P^{2+} was 1.32×10^{16} P^{2+} ions/cm^2 and for Sr^{2+} it was 0.2×10^{16} Sr^{2+} ions/cm^2). Because of the O_2 partial pressure, TiO_2 and CaO have been formed onto the Ti substrate during implantation, resulting in the sputtering yield dropping below one (the number of sputtered ions is less than the implanted ions). Similar was the case for P^{2+} ions that formed PO_4, and Sr^{2+} ions formed SrO in the process of O_2 backfilling. Subsequent heating of the implanted Ti substrate at 80°C for 3h, Ca and Sr react with O_2 and H_2O, forming $Ca(OH)_2$ and $Sr(OH)_2$. In this condition, the surface contains CaO, SrO, Ca $(OH)_2$ and Sr $(OH)_2$ as the major components implanted in the TiO_2 matrix. In the present phase, these finely dispersed amorphous phases are in a ready-to-react form for the synthesis of SrHA in

subsequent annealing. After annealing this implanted Ti substrate at 600°C for 5 min in a fast-annealing furnace, a crystalline phase of SrHA was produced. Annealing the Ti substrate had three beneficial effects: the first one was the formation of SrHA, the second one was conversion from an amorphous phase to a crystalline phase, and the third advantage was to overcome the implantation damage. Since amorphous SrHA has detrimental effects in a Ti implant surrounded by body tissues, the present crystalline form of SrHA is beneficial for bioimplant applications.[26,27]

Ag^{2+} ions of energy 100 KeV were implanted on the as-formed SrHA ion-implanted Ti surface with a concentration as low as 1.1×10^{15} ions/cm^2 that can act as an antibacterial agent. The Ag^{2+} ions were implanted at a depth of 35 nm from the surface of Ti. The whole process of implantation of Ca^{2+}, P^{2+}, Sr^{2+}, and Ag^{2+} ions was carried out over a span of 196 hours, excluding the post-implantation treatments.

Depth Profile Analysis

The maximum depth profile was measured at 70 nm, 69 nm and 75 nm for Ca^{2+}, P^{2+}, and Sr^{2+} ion implantation, respectively, whereas the maximum range approached 30 nm, 32 nm, and 30 nm for Ca^{2+}, P^{2+}, and Sr^{2+} ion implantation as depicted in Figures 1–3 respectively. The depth profile calculations were carried out by SRIM software.[28] Under modified vacuum conditions, the depth profiles of the implanted ions were drastically changed.

Preparation of [SrHA-Ag/Ti (LTHSC)) and (SrHA-Ag/Ti (CD)]

The LTHSC technique was used to coat the cpTi surface with Ag-SrHA powder, which had been prepared through a wet chemical process. A straight cylindrical nozzle was used to discharge nitrogen gas, released from a cylinder operating at 10^{-3} torr, known as the carrier gas. The SrHA powder was introduced into a powder hopper, which was then carried by a nitrogen carrier gas. The gap between the nozzle and the substrate was maintained 1 cm apart. Allowing the Ag-SrHA powder to collide with the cpTi surface via the spray nozzle resulted in the formation of Ag-SrHA coating layers.[29] Similarly, Ag-SrHA deposition on cpTi was carried out using electrochemical deposition as described in the literature.[30,31]

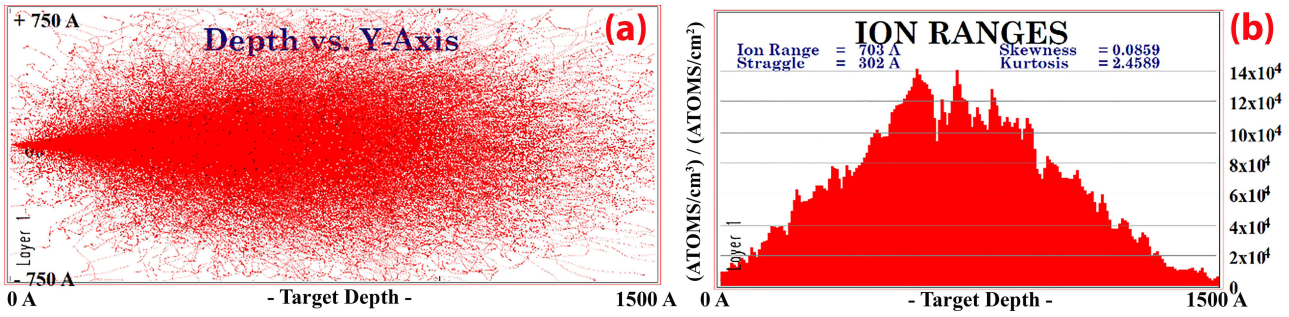

Figure 1 (**a**). Depth distribution of Ca ions inside the Ti and (**b**) range of ions inside Ti.

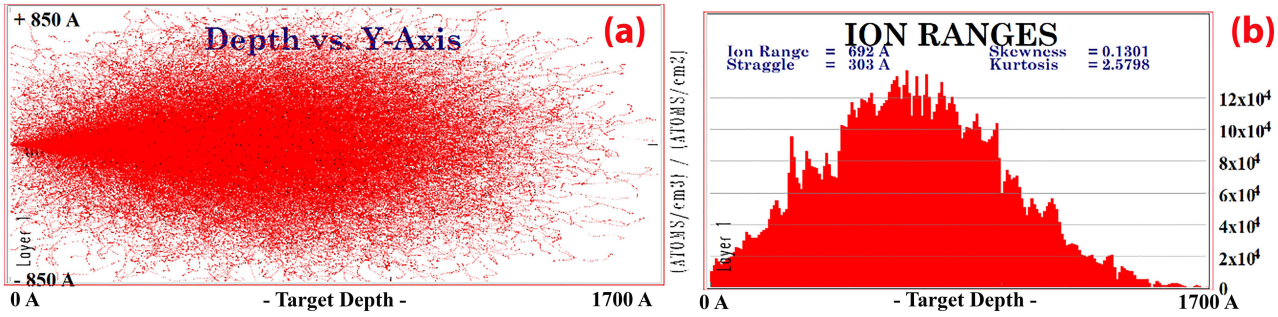

Figure 2 (**a**). Depth distribution of P ions inside Ti and (**b**) range of ions inside Ti.

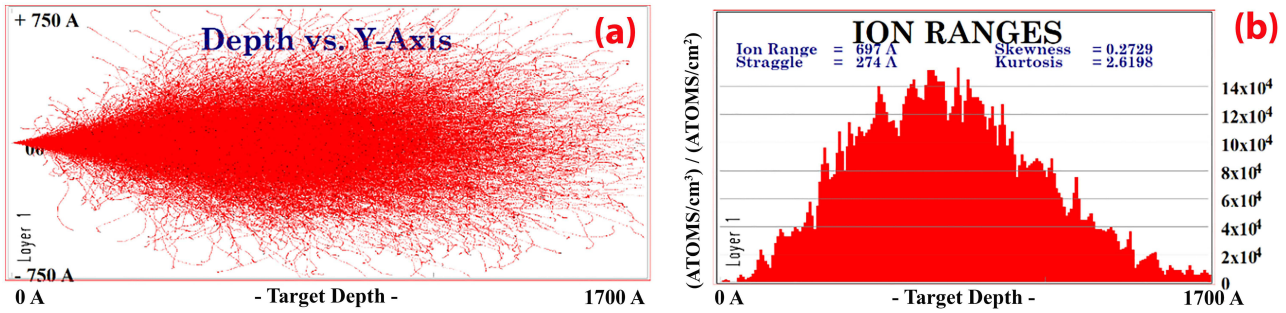

Figure 3 (**a**). Depth distribution of Sr ions inside Ti and (**b**) range of ions inside Ti.

The present investigation focuses on the synthesis of Ag-incorporated SrHA on a Ti substrate, their adhesion strength and biological behaviour. So, in comparative analysis, only the biological studies pertaining to CD and LTHSC specimens have been carried out.

Physical Characterization

Scanning Electron Microscope (SEM)

Using a scanning electron microscope (SEM, JSM-6700FM, JEOL, Japan), the morphological characteristics of the cpTi surface and SrHA-Ag/Ti (ion-implanted) have been examined.[4]

X-Ray Photoelectron Spectroscopy (XPS)

The elemental profile of ion-implanted Ti surface was determined by employing XPS (MICROLAB-350, Britain) with A1-Kα (1486.6 eV) as the excitation source.[32]

Fourier Transform Infrared Spectroscopy (FTIR)

Bruker FTIR Spectrophotometer (Alpha model) was used to conduct Fourier Transform Infrared Spectroscopy (FTIR) on the as-formed specimens to determine the functional groups of the coating composition. An infrared (IR) beam is reflected from the titanium surface at various (almost close to glancing) angles of incidence as part of the measuring procedure. Two different IR beams were used to record the spectrum: one polarised perpendicular and the other polarised parallel to the surface of the mounted specimen. On the basis of the ratio of S to N (signal-to-noise ratio), multiple averaged computer scanning was performed for the specimen during the data-acquiring process. At a resolution of 4 cm^{-1}, the spectra have been obtained in the spectrum of 4000–400 cm^{-1}; all generated spectra have been computed with double-digit accuracy.[33,34]

Contact Angle

Measurement of the contact angle of the as-formed specimens with simulated body fluid (SBF) at pH 7.2 and Dulbecco's modified eagle's medium (DMEM) (cell culture media) was carried out using the contact angle setup (VCA optima, USA). The angle of contact of the stationary liquid droplets with the specimen substrates was quantified.[35]

Adhesion Strength

The adhesion strength of the coatings on the specimens was assessed using a universal material testing machine (CMT4204, Sans Material Test Instruments Co., Ltd.) at a crosshead speed of 2 mm/min. Maximum load was measured when the coating was peeled out of the substrate. The adhesion strength (σ) was determined using the following formula:

$$\sigma = F/a,$$

where "a" is the contact area of the coating with the stainless steel substrate, and F is the highest load when the coatings were peeled.[32]

Cell Culture

MC3T3-E1 pre-osteoblast cells (NCCS, Pune) were cultured in DMEM (GIBCO) medium supplemented with 10% fetal bovine serum (GIBCO), 100 mg mL^{-1} of streptomycin, and 100 units mL^{-1} of penicillin. The mixture was then incubated in a humidified atmosphere with 5% CO_2 at a temperature of 37°C. The cultured media was replaced with fresh media to eliminate non-adherent cells on every alternative day for two weeks.[36]

Live/Dead Osteoblast Cell Analyses

The viability of MC3T3-E1 pre-osteoblast cells was determined using a Live and Dead viability/Cytotoxicity Kit (Molecular Probes, USA). Then the specimens were incubated for 7 days in standard culture conditions and were washed 3 to 4 times and treated with 2.5% glutaraldehyde (Solarbio Company, Beijing, China) solution for 2h at 4°C. The specimens were then transferred to a new 24-well plate. After rinsing with PBS twice, they were left to stain at room temperature in a dark environment. Again, the specimens were added with 1 mL of a prepared solution (consisting of 2 µM calcein AM and 4 µM EthD-1) and incubated for 10 min in the dark. The fluorescence microscope (Olympus, Tokyo, Japan) was used to analyze the Live/Dead osteoblast cells qualitatively.[37]

Osteoblast Cell Viability Test by MTT Assay

The cell viability was assessed by culturing them on specimens for 1, 7, and 14 days. The MTT (3-(4,5-dimethylthiazol-2-yl)-2,5-diphenyltetrazolium bromide) assay was used to quantify the functionality and viability of mitochondria in the cells. The tetrazolium salt MTT undergoes conversion by mitochondrial succinic dehydrogenase of live cells, resulting in the formation of a dark-blue insoluble compound known as formazan. A solution of MTT (5 mg/mL, Sigma Aldrich) was added to each well, and the cells were incubated at 37° C for 4 h. After the removal of growth media, dimethyl sulfoxide (DMSO) was put into each well to facilitate the dissolution of cells. Cell viability was determined by quantifying the optical density of the coloured substance in the solution using a spectrophotometer (Microplate Reader EL 308; Bio-Teck Instrument, Winooski, VT) which was configured to measure at a wavelength of 450 nm. The blank reference was extracted from wells without cellular structures.[29,38]

Gene Expression Using Quantitative Real-Time Polymerase Chain Reaction (qRTPCR)

The osteogenic gene expression of MC3T3-E1 pre-osteoblast cells was assessed using a real-time polymerase chain reaction (qRT-PCR; Bio-Rad Laboratories) to quantify the mRNA expression of marker gene levels such as Runt-related transcription factor 2 (RUNX2), type-1 collagen (COL1), and osteocalcin (OCN). To extract RNA, cells were seeded at a density of 4×10^4 cells/well for 1, 7, and 14 days, then lysed with TRIzol (Invitrogen). Using a superscript II first-strand cDNA synthesis kit (ThermoFisher), 1 mg of RNA was reverse-transcribed into complementary DNA (cDNA).[39] The forward and reverse primer sequence has been depicted in Table 1.

Bacterial Viability

The antibacterial properties of composites were tested using *S. aureus*, the most prevalent gram +ve bacteria that causes osteomyelitis. Bacteria viability was evaluated using the MTT test in vitro. The bacteria were cultured in a Mueller-Hinton Broth (MHB) medium. After that, the as-formed specimens were incorporated into the centre of a 24-well plate and put in a CO_2 incubator at 37°C with 1 mL of 1×10^6 CFU/mL bacterial suspension in each well. The bacteria culture

Table 1 Forward and Reverse Primer Sequences

Gene	Forward Primer Sequence (5′–3′)	Reverse Primer Sequence (5′-3′)
COL I	CCCCAGCCACAAAGAGTCTA	GGATCATCCACGTCTCGTTT
OCN	CTGAGAGGAGGAAGCACCAT	CCATCCTCATACCTGCACCT
RUNX2	CACCGAGACCAACAGAGTCA	TGCTTGCAGCCTTAAACTGA

was carried out for time periods of 10 h, 20 h and 30 h, and the adherent bacteria were evaluated for bacteria viability test by adding 150 µL bacteria suspension with 150 µL MTT solution (5 mg/mL) and incubated at 37°C for 6 h. The experiment was conducted three times for each test. The bacterial viability was assessed by measuring the optical density (OD) of the substrate solution.[40]

Statistical Analysis

The experiments were performed (n = 3 for contact angle and adhesion strength and n = 5 for other biological studies), and the outcomes were expressed as mean ± standard deviation for the synthesized coatings. The statistical analyses were conducted using one-way Analysis of Variance (ANOVA) with Tukey's multiple comparison tests (Prism, version 5.0). A significance level of $p < 0.05$ was chosen to determine the statistical significance of the observed differences between the groups.

Results

Scanning Electron Microscopy Study

The morphological attributes and surface nano topography of (a) cpTi, as well as (b) SrHA-Ag/Ti (ion-implanted) were illustrated in SEM micrographs (Figure 4). Both the cpTi and SrHA-Ag/Ti (ion-implanted) surface exhibited almost similar surface nano topography with visible coating in the later surface.

X-Ray Photoelectron Spectroscopy Study

With the aid of XPS, the elemental profile of the surface was estimated, and elements, such as Ca, P, Sr, Ti and O were detected (Figure 5).

Fourier Transform Infra-Red Spectroscopy Study

FTIR spectrum showed the formation of SrHA with several unique absorption peaks as shown in Figure 6. The PO_4^{3-} (544 cm^{-1}, 614 cm^{-1}, and 1033 cm^{-1}) and OH^- (1654 cm^{-1} and 3491 cm^{-1}) functional groups are ascribed to the presence of SrHA.

Contact Angle

The contact angles of the synthesized specimens were quantified using two separate measuring fluids, DMEM and SBF. The results were then compared to cpTi, as depicted in Figure 7. The ion-implanted SrHA-Ti demonstrated a reduced angle of 35° and 40° in SBF and DMEM. The contact angles for the cathodically deposited SrHA-Ti and LTHSC deposited SrHA-Ti implants were 43°, 41° for SBF and 45°, 49° for DMEM, respectively.

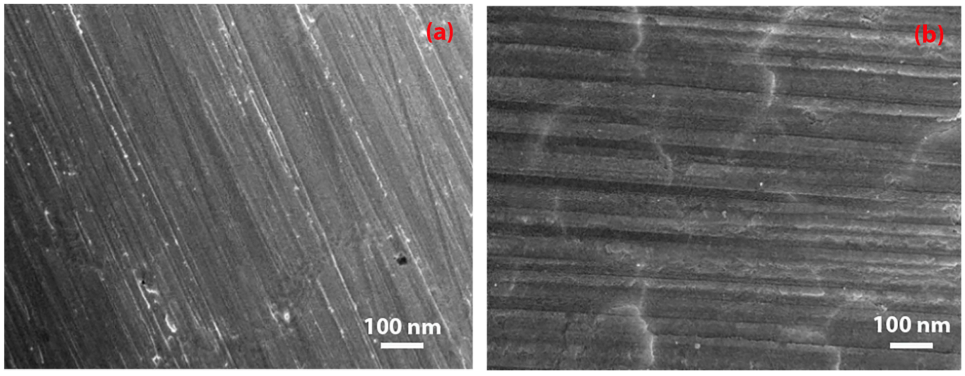

Figure 4 Morphological attributes and surface nano topography of (**a**) cpTi, as well as (**b**) SrHA-Ag/Ti (ion-implanted).

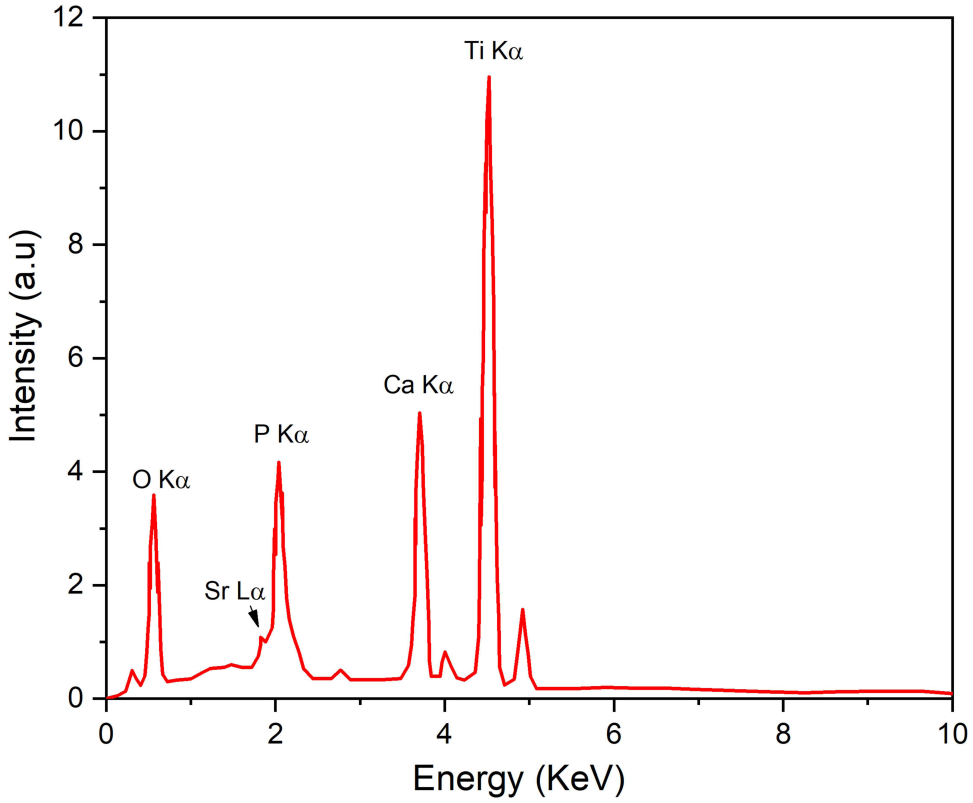

Figure 5 The elemental composition of ion-implanted Ti spectrum using XPS.

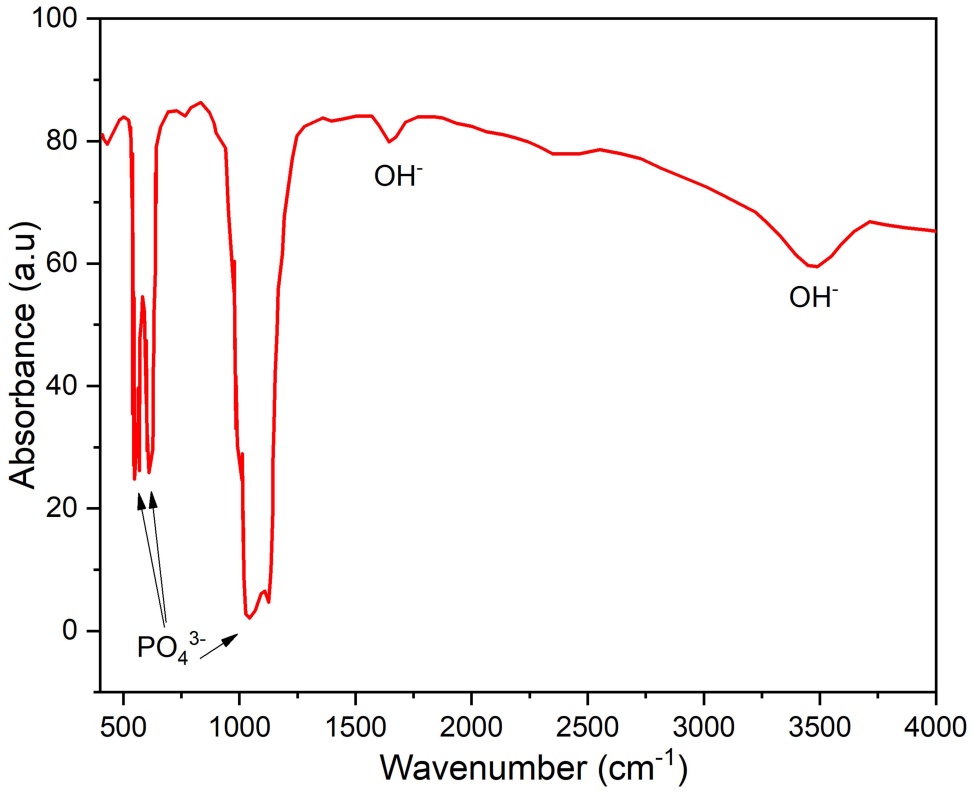

Figure 6 FTIR spectrum of as-fabricated specimen.

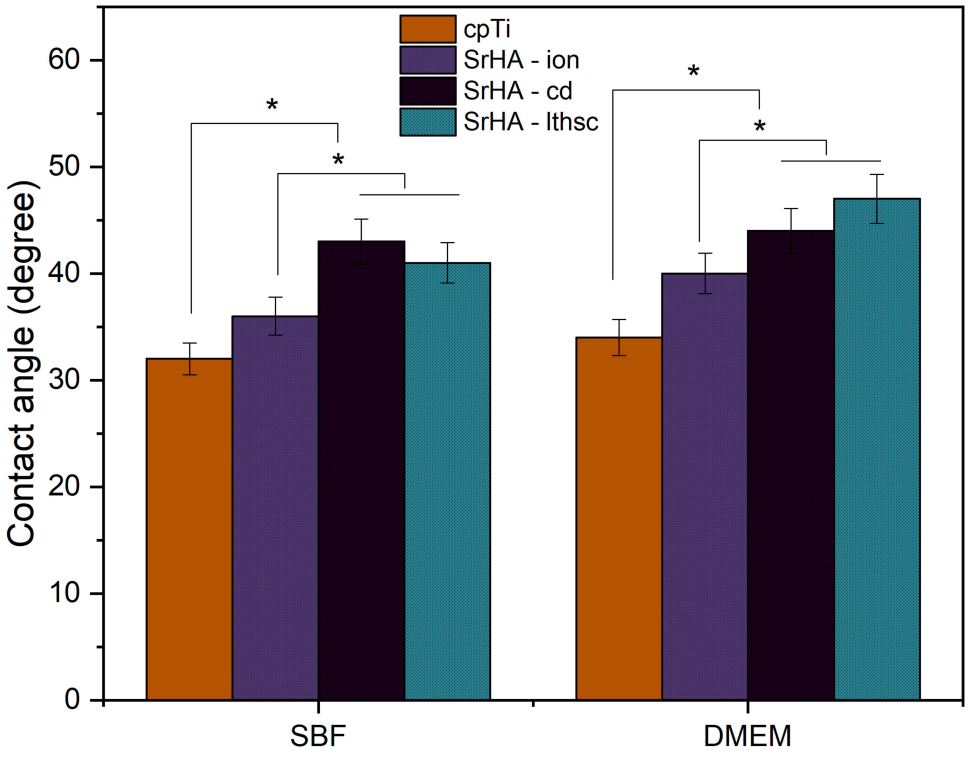

Figure 7 Contact angle of as-fabricated specimen. *$p < 0.05$, denotes a significant difference.

Adhesion Strength

The adhesion strength of the ion-implanted specimen was 43 ± 2.3 MPa, while that of the specimen with cathodic deposition had an adhesion strength of 6.3 ± 0.31 MPa, and the LTHSC deposited specimen showed a strength of 19 ± 0.92 MPa. The adhesion strength of the ion-implanted specimen was found to be significantly higher than the other two specimens (Figure 8).

Cell Proliferation

The MTT assay was used to evaluate cell proliferation on the specimens at 1, 7, and 14 days of incubation (Figure 9). The as-formed specimens had significantly higher cell proliferation than cpTi at all points of the incubation period. The cell proliferation on the SrHA-Ag/Ti (ion-implanted) surface was considerably higher than that of SrHA-Ag/Ti (CD) and SrHA-Ag/Ti (LTHSC). However, there was no significant difference in cell viability between SrHA-Ag/Ti (CD) and SrHA-Ag/Ti (LTHSC) specimens.

Bacterial Viability

The antibacterial activity was assessed by examining the viability of *S. aureus* (Figure 10). Antibacterial efficacy was measured after incubating the Ag-incorporated SrHA specimens at 37°C for 24h. On Ag-incorporated SrHA, the viability of *S. aureus* was reduced by around 40–60%. The presence of Ag in the Sr-HA ion-implanted surface resulted in a decrease in *S. aureus* by about 60%, indicating a similar pattern of 40% and 30% reduction, respectively, in specimens synthesized by cathodic and LTHSC deposition.

Live/Dead Cell Fluorescence Analysis

The qualitative Live/Dead cell analyses of the as-formed coatings were visualized using a fluorescence microscope to understand the activities of osteoblast survival status (Figure 11). It was found that a number of MC3T3-E1 cells had grown on all specimens as the culture time increased, suggesting that the SrHA surfaces induce a conducive environment for cell adherence, differentiation and proliferation.

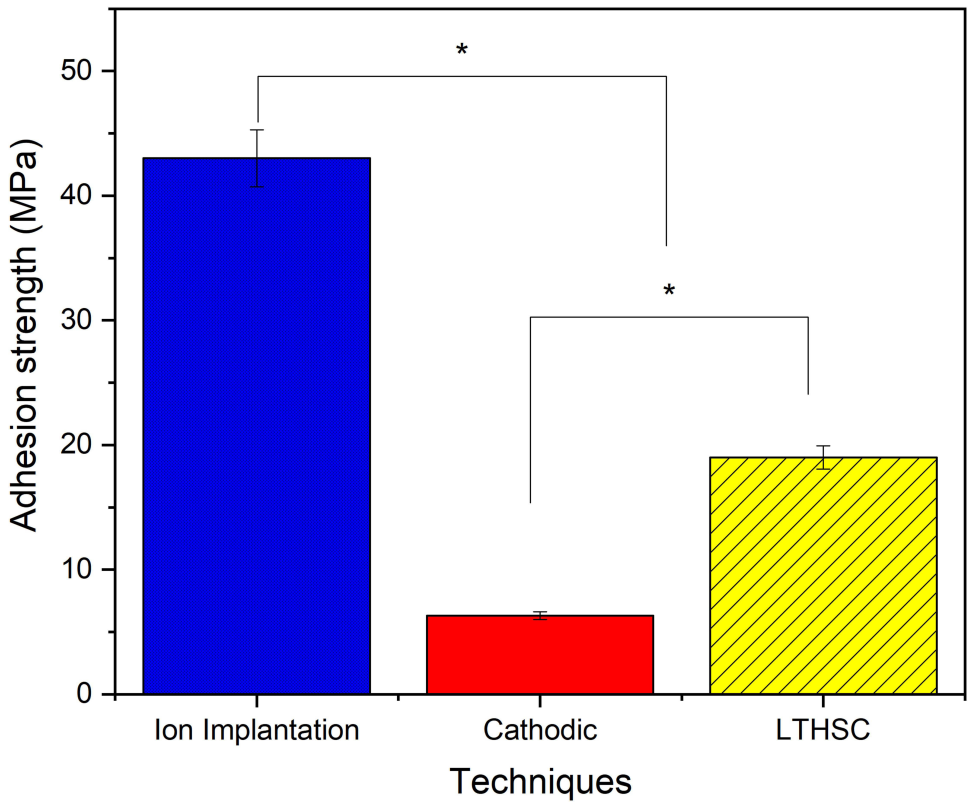

Figure 8 Adhesion strength of as-fabricated coatings. *$p < 0.05$, denotes a significant difference.

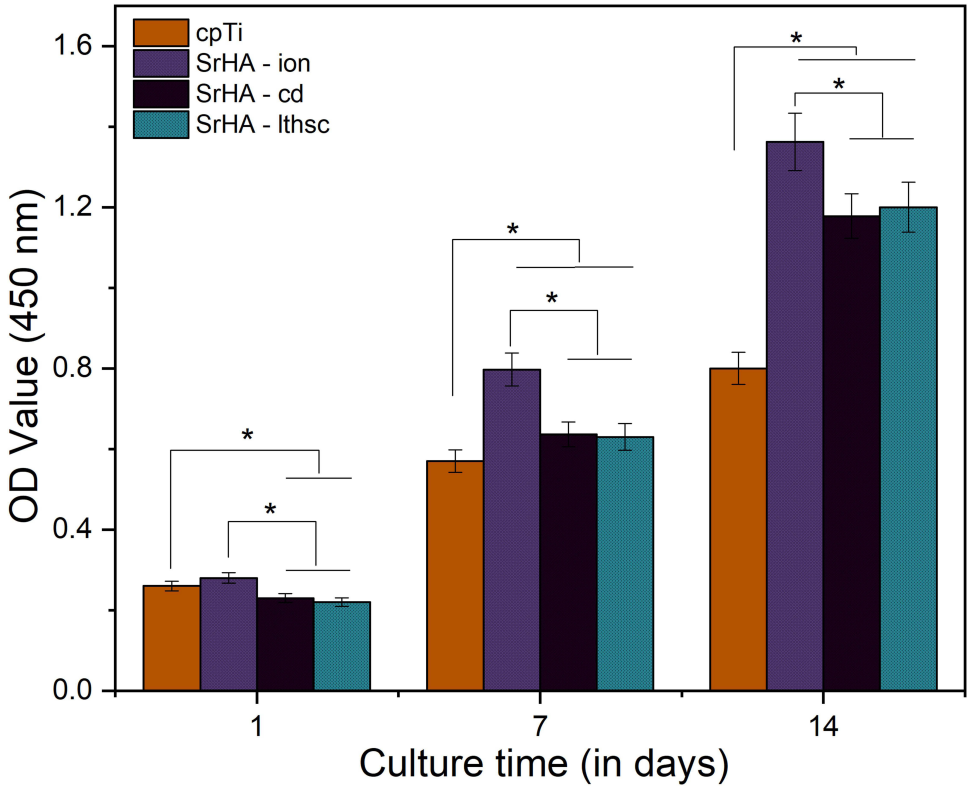

Figure 9 MTT assay using osteoblast cells. *$p < 0.05$, denotes a significant difference.

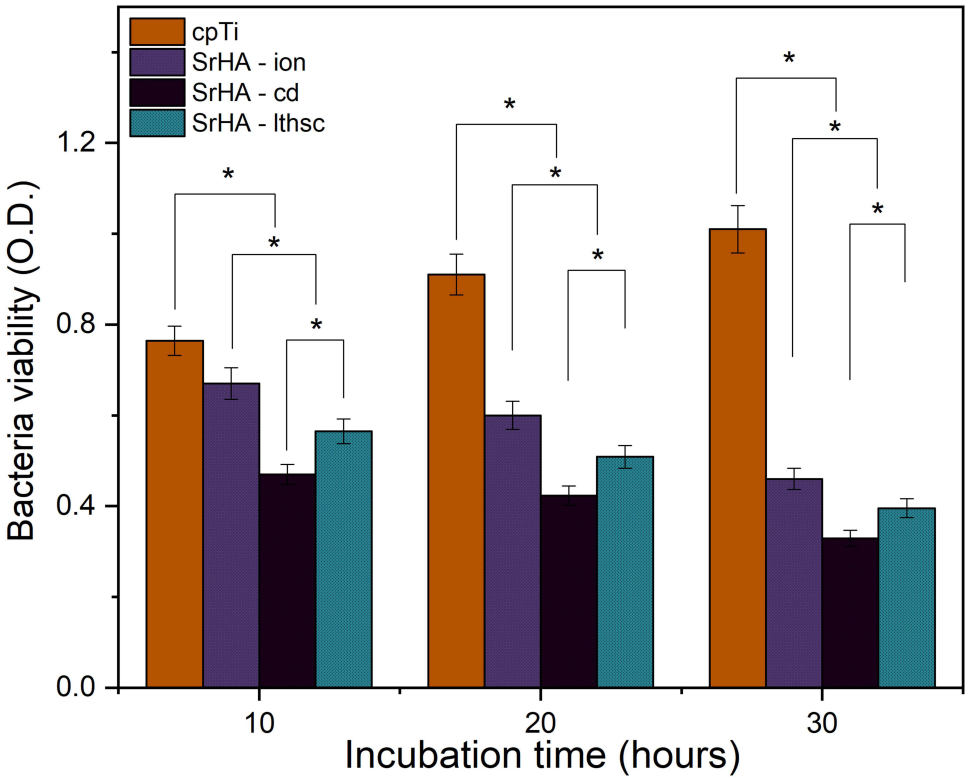

Figure 10 Bacteria viability on as-fabricated specimens. *$p < 0.05$, denotes a significant difference.

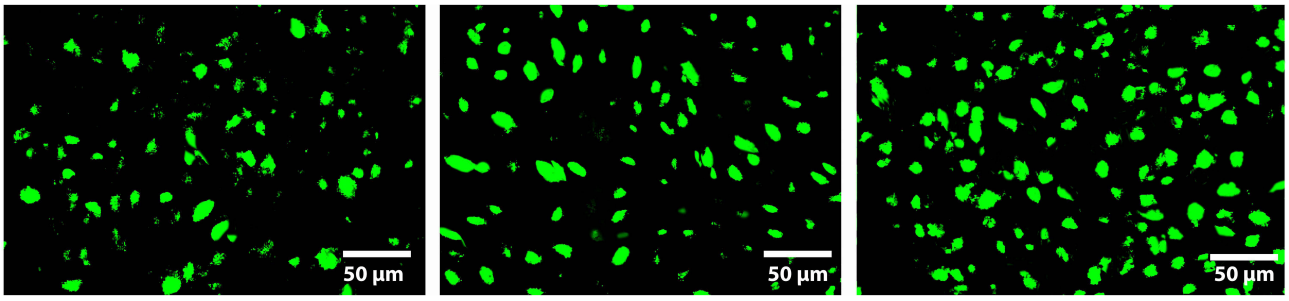

Figure 11 Fluorescence micrographs of osteoblast cells after 7 days of culture.

Gene Expression Studies Using qRT-PCR

The levels of gene expression associated with osteogenesis on the as-formed specimens were assessed using qRT-PCR (Figure 12). The number of viable osteoblast cells on all the as-formed specimens on days 7 and 14 was significantly high ($p > 0.05$). As seen in Figure 12a, on day 1, gene expression of RUNX2 of SrHA-Ag/Ti (ion-implanted) was significantly higher than the control cpTi and the coating deposited by CD and LTHSC techniques. However, on day 7, no noticeable difference was observed among the as-formed specimens along with the control cpTi. On day 14, SrHA-Ag/Ti (ion-implanted) specimen exhibited significantly higher RUNX2 gene expression than others. Further, on day 14, gene expressions of OCN (Figure 12b) and COL1 (Figure 12c) were significantly high on day 14, and there was a significant increase in the expression of the OCN gene on SrHA-Ag/Ti (ion-implanted) that leads to improved osseointegration.

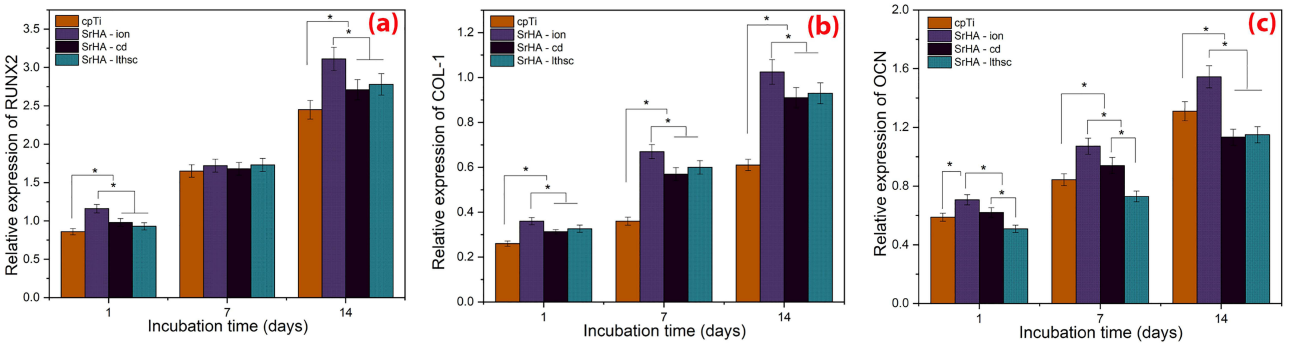

Figure 12 Analysis of osteogenic relative gene expressions of (**a**) RUNX2, (**b**) COL1, and (**c**) OCN. *$p < 0.05$, denotes a significant difference.

Discussion

Prior studies have investigated the efficacy of ion implantation as a method to enhance the osseointegration of Ti implants. However, surface treatments have mainly focused on modifying surface properties, including surface chemistry, roughness, and energy. Therefore, it is essential to optimize the biological and mechanical properties of a metallic implant to obtain an ideal bioimplant surface.[41] Although plasma spray is a state-of-The-art technique for surface modification of Ti implants, it has several disadvantages that include various phases of calcium phosphate in the coating, giving rise to surface delamination and changes in the crystal structure of the matrix, subsequently releasing the coated nanoparticles that may cause inflammatory reactions.[42] To overcome these drawbacks of plasma spray, the conventional ion implantation technique has been utilized in the present study, which is supposed to unalter the nano-topography patterned on the Ti surface without changing its surface chemistry.[13,43] The primary drawback of conventional ion implantation is that it is a line-of-sight process limited to the implantation of two-dimensional surfaces. However, with the use of a rotating sample holder, this problem has been largely solved in the present investigation.[44] Ion implantation technique has not been found to affect the texture of the surface. Nano-topographies may directly correspond to the size of protein and membrane receptors, which could enhance osteoblast differentiation and tissue regeneration.[45] On the other hand, considering the importance of nano-topographical features, the synergistic effects of dual-length scale materials show promising results in improving osseointegration.[46]

In the present investigation, once the coating was formed on the patterned surfaces using cathodic and LTHSC techniques, the nano-topographic patterns were concealed by the Ag-SrHA coating formed on them.[47] On the other hand, in the ion implantation technique, the coating formed was a gradient layer conglomerated with the composition of the patterns as well as underneath the cpTi surface.[48–50] Thus, the efficacy of nano-topography patterned surfaces in interacting with the osteoblasts is retained. These treatments bring out changes in surface topography by a sputtering process while leaving the surface chemistry unaltered.[51] On the other hand, the gradient layer accounts for the high adhesion strength of the coating, giving rise to a coating with long-term stability. This study has investigated the impact of nano-topography patterned surfaces on osteoblast and bacteria cells after impregnating these surfaces with osteogenic and antibacterial agents using ion implantation technique, and the biological studies on this surface have been compared with Ag-SrHA coated specimens synthesized by cathodic deposition[30] and LTHSC technique.[29]

It was evident from the XPS spectrum that SrHA-Ag coatings have been formed on the nano-topography patterned cpTi surfaces. While in both CD and LTHSC techniques, Ag^{2+} and Sr^{2+} have substituted the Ca site of HA inside the apatite lattice, Ag^{2+} has been flash-coated on ion-implanted SrHA coating. Since Sr and Ca have similar chemical and physical properties, substituting Sr at the Ca site in HA is an elementary procedure. Subsequently, the FTIR result validated the presence of PO_4^{3-} and OH^- band peaks, as depicted in Figure 6. The peaks associated with the PO_4^{3-} group resulted from the symmetrical P–O stretching, while the peaks assigned to the OH^- group were generated due to the stretching modes of O–H bands.[52,53] Apart from the PO_4^{3-} and OH^- groups, no impurities or additives were detected, indicating that the HA phase has been formed. Moreover, depth analysis using SRIM software[9,54] demonstrated that several ranges of gradient layers were formed on the cpTi surface by the deposition of Ca^{2+}, Sr^{2+}, and P^{2+}. Even though

the dosis of the ions were calculated to obtain (Ca+Sr)/P ratio of 1.67, from proton-induced X-Ray emission (PIXE)[55] spectroscopic analysis, the (Ca+Sr)/P ratio was found to be 1.615, which is almost close to the ideal Ca/P ratio (1.67) of HA.

On the other hand, surface wettability is one of the most important attributes that affect cell adhesion, protein adsorption, blood coagulation, platelet adhesion/activation, and tissue growth for biomedical applications.[56] It is an important factor in the evaluation of hydrophilic characteristics and, therefore, the attachment and proliferation of osteoblast cells. It has been found that surface roughness may impact hydrophilicity, which is a crucial factor for the nucleation and cell development events that lead to osseointegration.[57,58] The key findings of this study indicate that the surface of the SrHA-Ag/Ti (ion-implanted) specimen is mostly hydrophilic in nature as compared to the other two modified surfaces, such as SrHA-Ag/Ti (CD) and SrHA-Ag/Ti (LTHSC). The decreased contact angle of the SrHA-Ag/Ti (ion-implanted) may be attributed to the effect of nano-topography patterned surface that remains intact even after ion implantation. Moreover, the drawback associated with acetabular displacement is the interfacial bonding strength between the substrate and the implant.[22,59] As per ASTM standard F1147, the minimum tensile strength of a Ca-P coating must be 34.5 MPa, and it has been achieved only by the ion implantation technique.[60] Upon analyzing the adhesion strength, it was observed that the specimen obtained through ion implantation exhibited the maximum bonding strength when compared to the specimens obtained using CD and LTHSC techniques. Moreover, in the ion implantation technique, the implanted ions form a gradient layer inside the Ti matrix. Hence, surface delamination problems do not arise. The presence of nano-topography patterns in the SrHA-Ag/Ti (ion-implanted) surface enhances the interface adhesive force between the cpTi surface with osteoblast cells. Although all three investigations assessed the antibacterial properties of Ag^{2+} ions and osteogenicity through the formation of osseous tissues by MC3T3-E1 cells cultured on SrHA-Ag/Ti surface, ion implantation techniques exhibited superior properties.

For developing novel coatings having both antibacterial and pro-osteogenic characteristics, bi-functionalization of Ti implants has been adopted. The deposition of osteogenic agents on Ti implants favours surface osteogenic properties.[61] Several in vitro investigations have shown that Sr promotes bone formation by activating the calcium-sensing receptor and inhibiting bone resorption by uplifting osteoprotegerin (OPG) and reducing receptor activators of nuclear factor kappa β ligand (RANKL).[40,62] OPG, a protein generated by osteoblasts, inhibits RANKL-induced osteoclastogenesis by acting as a RANKL decoy receptor. The OPG/RANKL ratio consequently plays a key role in regulating bone resorption and osteoclastogenesis. The calcium-mimicking structure of Sr stimulates the CaSR/PI3K/Akt signal pathway, preventing GSK3 production. This promotes the expression, nuclear localization, and transcriptional activity of β-catenin. Additionally, Sr may enhance the expression of RUNX2, ALP, OCN, and COL1 via upregulating Wnt5a pathway.[63] The antibacterial properties, along with osteogenicity, are important parameters for an implant to be used for acetabular fracture. Ag is a broad-spectrum antibacterial and antifungal agent that can even inhibit *methicillin-resistant S. aureus s*trains.[64] It has been reported that AgNPs can readily act against bacterial cells more effectively than their micron-sized counterparts. Moreover, the size and shape of the AgNPs play a major role in bactericidal action. Morones et al[65] reported that AgNPs of 1–10 nm diameter exhibited optimum bactericidal action.[66] From recent studies, it has been observed that the nano-Ag released from the surface of the implant penetrates the bacterial cell walls, which leads to membrane damage, and subsequently interacts with sulfur and phosphorus-containing biological components, including DNA, RNA, proteins, and enzymes by resulting in the production of reactive oxygen species (ROS). Increased ROS induces an apoptosis-like response, DNA damage, and lipid peroxidation, ultimately resulting in the death of the bacteria.[67] However, its application in the biomaterials field was compromised because of its cytotoxicity resulting from excess concentrations of Ag. Additionally, it should be considered that higher concentrations of Ag might have cytotoxic effects on mammalian cells. A maximum concentration of 0.7% of Ag has been found to be non-toxic for biomedical implants.[68] Hence, in the present investigation, we have taken the concentration of Ag to be 0.5%. According to the bacterial viability results, SrHA-Ag/Ti (CD) showed reduced bacterial cell viability as compared to SrHA-Ag/Ti (ion-implanted) and SrHA-Ag/Ti (LTHSC) surfaces. CD and LTHSC specimens resulting in lower bacterial viability may be ascribed to the presence of Ag in HA lattice structure, which leads to better antibacterial activity. On the other hand, ion-implanted specimens involve flash coating Ag on its surface resulting in comparatively lower antibacterial activities. This may be due to less available Ag ions because of their attachment to the Ti lattice. Moreover, since the Ag ions were

implanted in the near-surface regions of Ti, there would be a higher loss of these ions by sputtering, giving rise to less available Ag. However, the release of Ag persisted spontaneously from the specimens prepared by other techniques.

To investigate cell differentiation, certain gene markers were investigated such as COL1, which primarily contributes to the extracellular matrix (ECM) of bone; RUNX2, which is expressed during osteoblast formation; and OCN, which is a late indicator of osteogenic differentiation.[68] The current investigation provided strong evidence that all of the markers for osteogenic gene expression were significantly higher in the SrHA-Ag/Ti (ion-implantation) specimen than in the other two modified surfaces. Braux et al discovered that the presence of Sr^{2+} ions stimulates the growth of human primary bone cells. Furthermore, the osteogenic gene expression in the presence of Ag ions indicates that the cytotoxic effect of the Ag ions did not affect the osteoblast cells.[69] Additionally, the MTT assay study confirmed that there is an increase in cell viability on all three substrates (SrHA-Ag/Ti (CD), SrHA-Ag/Ti (LTHSC), and SrHA-Ag/Ti (ion-implanted)), exhibiting their cytocompatibility nature. In a similar study, Lee et al[29] found that there was no significant difference in cell proliferation between the control (Ti) and the HA-coated Ti surfaces via the LTHSC technique. Additionally, a study by Lafzi et al,[70] measured osteogenic gene expression in MC3T3-E1 cells on nano-HA-coated Ti substrates. Their results showed better expression on day 7 as compared to day 14, suggesting better gene expressions. Another study demonstrated that SrHA-Ag coatings, along with silicon co-doping, exhibited superior biological characteristics as compared to HA and HA-Ag coatings while maintaining similar anti-bacterial effects on HA-Ag coating.[71] The live/dead fluorescence staining on all the specimens exhibited their cytocompatible nature, and Ag is shown to have the least effect on the growth of osteoblast cells. Simultaneously, it can be observed that there is the highest number of live cells in the SrHA-Ag/Ti (ion-implanted) specimen. Therefore, the surfaces that were ion-implanted with SrHA-Ag/Ti were found to be suitable for cell adhesion and proliferation. Geng et al discovered that Sr doping to the HA coating layer on Ti implants can mitigate the cytotoxicity of Ag incorporated into the coating. By stimulating the osteoblasts and inhibiting the osteoclasts, the later is also known to disrupt the process of osteogenesis when incorporated. Nevertheless, the replacement of Sr in Ag/SrHA nanoparticles may effectively mitigate the adverse consequences of Ag and amplify the biological efficacy of HA. Therefore, the synthesized Ag/SrHA nanoparticles have the potential to be used in biomedical implants, specifically in orthopaedic and dental applications, due to their exceptional ability to promote bone growth and prevent bacterial infections.[72,73] The study demonstrated that the nano-scale pattern of the Ti surface has strong mechanical interlocking capability with surrounding bone, which may enhance the stability of the implant as compared to smooth surfaces. Moreover, the presence of nano/micron-patterned surface roughness enhances the process of protein adsorption, promotes the attachment of osteoblasts, helps in the development of osteoblasts into bone cells, and facilitates the integration of implants with surrounding bone tissues in living organisms.

Conclusions

In the present study, Ca^{2+}, P^{2+}, and Sr^{2+} were implanted into a nano-topography patterned Ti surface to synthesize Sr-HA/Ti; Ag was subsequently implanted on the as-formed specimen as a flash antibacterial coating. The surface topography of the ion-implanted surface retained its initial structure. The SrHA-Ag coating exhibited optimal osteoblast function while concurrently minimizing bacterial adherence. The inclusion of Ag in the SrHA coating showed a more effective ability to prevent infection caused by *S. aureus* bacteria. The presence of Sr had a beneficial effect on the surface of SrHA-Ag, leading to a considerable improvement in the attachment, proliferation, and differentiation of MC3T3-E1 cells. The adhesion strength of the ion-implanted coating was superior to the other two coatings and in accordance with ASTM standard protocol. Due to its enhanced adhesion, cytocompatibility, and strong antibacterial capabilities, SrHA-Ag/Ti (ion-implanted) may exhibit great promise for treating infectious bone defects and promoting the integration of bone to implant contacts in acetabular fossa defect sites. The findings of this research demonstrated that SrHA-Ag coating using the ion implantation method exhibits considerable promise as a viable substitute for the state-of-The-art plasma spray technique. The use of ion implantation to synthesize strontium-substituted hydroxyapatite is intriguing. Sr incorporation into HA can enhance bone regeneration and reduce osteoporosis risk. Combining SrHA with Ag^{2+} ions for antibacterial properties is novel. Few studies have explored this dual functionality. The synthesized specimens may be used as implant materials in critical body parts such as acetabular fracture sites, neurocranium or

viscerocranium sites, involving high-cost implant applications. Further research may be conducted on the large-scale production of cost-effective SrHA-Ag coatings that can be used as a common implant material.

Disclosure

The authors declare no conflicts of interest in this work.

References

1. Mears DC. Surgical treatment of acetabular fractures in elderly patients with osteoporotic bone. *J Am Acad Orthop Surg*. 1999;7(2):128–141. doi:10.5435/00124635-199903000-00006
2. Vanderschot P. Treatment options of pelvic and acetabular fractures in patients with osteoporotic bone. *Injury*. 2007;38(4):497–508. doi:10.1016/j.injury.2007.01.021
3. Li Y, Yang C, Zhao H, Qu S, Li X, Li Y. New developments of Ti-based alloys for biomedical applications. *Materials*. 2014;7(3):1709–1800. doi:10.3390/ma7031709
4. Swain S, Ong JL, Narayanan R, Rautray TR. Ti-9Mn β-type alloy exhibits better osteogenicity than Ti-15Mn alloy in vitro. *J Biomed Mater Res Part B Appl Biomater*. 2021;109(12):2154–2161. doi:10.1002/jbm.b.34863
5. Ronoh K, Mwema F, Dabees S, Sobola D. Advances in sustainable grinding of different types of the titanium biomaterials for medical applications: a review. *Biomed Eng Adv*. 2022;4:100047. doi:10.1016/j.bea.2022.100047
6. Swain S, Rautray TR. Ceramic coatings for dental implant applications. In: Gupta R, Motallebzadeh A, Kakooei S, Nguyen TA, Behera A, editors. *Advanced Ceramic Coatings for Biomedical Applications*. 2023:249.
7. Swain S, Rautray TR. Effect of surface roughness on titanium medical implants. In: Swain BP, editor. *Nanostructured Materials and Their Applications*. Singapore: Springer; 2021:55–80.
8. Shukur BN, Jassim RK. Evaluation of nano surface modification on CPTi dental implant using chemical method: mechanical and histological evaluation. *J Baghdad Coll Dent*. 2015;27(3):8–14. doi:10.12816/0015027
9. Rautray TR, Narayanan R, Kim KH. Ion implantation of titanium based biomaterials. *Prog Mater Sci*. 2011;56(8):1137–1177. doi:10.1016/j.pmatsci.2011.03.002
10. Bosco R, Beucken JVD, Leeuwenburgh S, Jansen J. Surface engineering for bone implants: a trend from passive to active surfaces. *Coatings*. 2012;2(3):95–119. doi:10.3390/coatings2030095
11. Gan L, Wang J, Pilliar RM. Evaluating interface strength of calcium phosphate sol–gel-derived thin films to Ti6Al4 V substrate. *Biomaterials*. 2005;26(2):189–196. doi:10.1016/j.biomaterials.2004.02.022
12. Narayanan R, Seshadri SK, Kwon TY, Kim KH. Calcium phosphate-based coatings on titanium and its alloys. *J Biomed Mater Res Part B*. 2008;85(1):279–299. doi:10.1002/jbm.b.30932
13. Wang G, Li J, Zhang W, et al. Magnesium ion implantation on a micro/nanostructured titanium surface promotes its bioactivity and osteogenic differentiation function. *Int J Nanomed*. 2014;9:2387–2398. doi:10.2147/IJN.S58357
14. Khatoon Z, McTiernan CD, Suuronen EJ, et al. Bacterial biofilm formation on implantable devices and approaches to its treatment and prevention. *Heliyon*. 2018;4(12):e01067. doi:10.1016/j.heliyon.2018.e01067
15. Swain S, Kwon TY, Rautray TR. Fabrication of silver doped nano hydroxyapatite-carrageenan hydrogels for articular cartilage applications. *bioRxiv*. 2021;1:2020.
16. Zhang YY, Zhu Y, Lu DZ, et al. Evaluation of osteogenic and antibacterial properties of strontium/silver-containing porous TiO2 coatings prepared by micro-arc oxidation. *J Biomed Mater Res Part B Appl Biomater*. 2021;109(4):505–516. doi:10.1002/jbm.b.34719
17. Garcia-Sanz FJ, Mayor MB, Arias JL, et al. Hydroxyapatite coatings: a comparative study between plasma-spray and pulsed laser deposition techniques. *J Mater Sci Mater Med*. 1997;8(12):861–865. doi:10.1023/A:1018549720873
18. Rautray TR, Kim KH. Nanoelectrochemical coatings on titanium for bioimplant applications. *Mater Technol*. 2010;25(3–4):143–148. doi:10.1179/175355510X12723642365322
19. Mohapatra B, Rautray TR. Strontium-substituted biphasic calcium phosphate scaffold for orthopedic applications. *J Korean Ceram Soc*. 2020;57(4):392–400. doi:10.1007/s43207-020-00028-x
20. Mishra S, Swain S, Rautray TR. Preparation of eggshell derived HA-BT composite for biomedical applications. *Integr Ferroelectr*. 2024;240(1):163–174. doi:10.1080/10584587.2023.2296316
21. Mangaraj S, Priyadarshini I, Swain S, Rautray TR. ZnO doped β-TCP ceramic-based scaffold promotes osteogenic and antibacterial activity. *Bio Bio Nano*. 2024;12:1–8. doi:10.1680/jbibn.23.00065
22. Rautray TR, Kim KH. Synthesis of Mg^{2+} incorporated hydroxyapatite by ion implantation. *Key Eng Mater*. 2013;529:114–118.
23. Anwar A, Kanwal Q, Sadiqa A, et al. Synthesis and antimicrobial analysis of high surface area strontium-substituted calcium phosphate nanostructures for bone regeneration. *Int J Mol Sci*. 2023;24(19):14527. doi:10.3390/ijms241914527
24. Rautray TR, Kim KH. Synthesis of controlled release Sr-hydroxyapatite microspheres. *InBioceramics-24*. 2012;1:1.
25. Ran L, Liu L, Gao J, et al. Strontium-doped hydroxyapatite and its role in osteogenesis and angiogenesis. *Int J Dev Biol*. 2023;67(4):137–146. doi:10.1387/ijdb.230091lc
26. Rautray TR, Narayanan R, Kwon TY, et al. Surface modification of titanium and titanium alloys by ion implantation. *J Biomed Mater Res Part B Appl Biomater*. 2010;93(2):581–591. doi:10.1002/jbm.b.31596
27. Behera DR, Nayak P, Rautray TR. Phosphatidylethanolamine impregnated Zn-HA coated on titanium for enhanced bone growth with antibacterial properties. *J King Saud Univ Sci*. 2020;32(1):848–852. doi:10.1016/j.jksus.2019.03.004
28. Ziegler JF, Biersack JP. The stopping and range of ions in matter. In: *Treatise on Heavy-Ion Science: Volume 6: Astrophysics, Chemistry, and Condensed Matter*. Boston, MA: Springer US; 1985:93–129.
29. Lee KW, Bae CM, Jung JY, et al. Surface characteristics and biological studies of hydroxyapatite coating by a new method. *J Biomed Mater Res*. 2011;98(2):395–407. doi:10.1002/jbm.b.31864

30. Swain S, Rautray TR, Narayanan R. Mg, and Co substituted hydroxyapatite coating on TiO_2 nanotubes formed by electrochemical methods. *Adv Sci Lett*. 2016;2(2):482–487. doi:10.1166/asl.2016.6888
31. Zhang Q, Leng Y, Xin R. A comparative study of electrochemical deposition and biomimetic deposition of calcium phosphate on porous titanium. *Biomaterials*. 2005;26(16):2857–2865. doi:10.1016/j.biomaterials.2004.08.016
32. Yuan Q, Xu A, Zhang Z, et al. Bioactive silver doped hydroxyapatite composite coatings on metal substrates: synthesis and characterization. *Mater Chem Phys*. 2018;218:130–139. doi:10.1016/j.matchemphys.2018.07.038
33. Barner BJ, Green MJ, Saez EI, Corn RM. Polarization modulation Fourier transform infrared reflectance measurements of thin films and monolayers at metal surfaces utilizing real-time sampling electronics. *Anal Chem*. 1991;63(1):55–60. doi:10.1021/ac00001a010
34. Mishra S, Rautray TR. Fabrication of Xanthan gum-assisted hydroxyapatite microspheres for bone regeneration. *Mater Technol*. 2020;35(6):364–371. doi:10.1080/10667857.2019.1685245
35. Swain S, Mishra S, Patra A, Praharaj R, Rautray TR. Dual action of polarised zinc hydroxyapatite-guar gum composite as a next generation bone filler material. *Mater Today Proc*. 2022;62:6125–6130.
36. Swain S, Koduru JR, Rautray TR. Mangiferin-Enriched Mn–Hydroxyapatite Coupled with β-TCP Scaffolds Simultaneously Exhibit Osteogenicity and Anti-Bacterial Efficacy. *Materials*. 2023;16(6):2206. doi:10.3390/ma16062206
37. Liu X, Chen C, Zhang H, et al. Biocompatibility evaluation of antibacterial Ti–Ag alloys with nanotubular coatings. *Int J Nanomed*. 2019;14:457–468. doi:10.2147/IJN.S193569
38. Swain S, Priyadarshini I, Rautray TR Osteogenicity and antibacterial property of polarized HA-UHMWPE composites as orthopedic implant biomaterial. *In*: *Asian Conference on Indoor Environmental Quality*; Singapore: Springer Nature: Singapore; 2021:59–69.
39. Swain S, Kumari S, Swain P, et al. Polarised strontium hydroxyapatite–xanthan gum composite exhibits osteogenicity in vitro. *Mater Today Proc*. 2022;62:6143–6147.
40. Swain S, Padhy RN, Rautray TR. Polarized piezoelectric bioceramic composites exhibit antibacterial activity. *Mater Chem Phys*. 2020;239:122002. doi:10.1016/j.matchemphys.2019.122002
41. Braceras I, Vera C, Ayerdi-Izquierdo A, et al. Ion implantation induced nano-topography on titanium and bone cell adhesion. *Appl Surf Sci Adv*. 2014;310:24–30. doi:10.1016/j.apsusc.2014.03.118
42. Gill BJ, Tucker RC. Plasma spray coating processes. *Mater Sci Technol*. 1986;2(3):207–213. doi:10.1179/mst.1986.2.3.207
43. Klymov A, Prodanov L, Lamers E, Jansen JA, Walboomers XF. Understanding the role of nano-topography on the surface of a bone-implant. *Biomater Sci*. 2013;1(2):135–151. doi:10.1039/C2BM00032F
44. Maitz MF, Poon RW, Liu XY, Pham MT, Chu PK. Bioactivity of titanium following sodium plasma immersion ion implantation and deposition. *Biomaterials*. 2005;26(27):5465–5473. doi:10.1016/j.biomaterials.2005.02.006
45. Boyan BD, Lossdörfer S, Wang L, et al. Osteoblasts generate an osteogenic microenvironment when grown on surfaces with rough microtopographies. *Eur Cell Mater*. 2003;6:22–27. doi:10.22203/eCM.v006a03
46. Zhang W, Wang G, Liu Y, et al. The synergistic effect of hierarchical micro/nano-topography and bioactive ions for enhanced osseointegration. *Biomaterials*. 2013;34(13):3184–3195. doi:10.1016/j.biomaterials.2013.01.008
47. Kim HN, Jiao A, Hwang NS, Kim MS, Kim DH, Suh KY. Nano-topography-guided tissue engineering and regenerative medicine. *Adv Drug Deliv Rev*. 2013;65(4):536–558. doi:10.1016/j.addr.2012.07.014
48. Swain S, Kumari S, Rautray TR. Bioceramic coating for tissue engineering applications. In: Gupta R, Motallebzadeh A, Kakooei S, Nguyen TA, Behera A, editors. *Advanced Ceramic Coatings for Biomedical Applications*. Vol. 23. 2023:197.
49. Swain S, Misra S, Rautray TR. Osteogenic trace element doped ceramic coating for bioimplant applications. In: Gupta R, Motallebzadeh A, Kakooei S, Nguyen TA, Behera A, editors. *Advanced Ceramic Coatings for Biomedical Applications*. 2023:293.
50. Priyadarshini I, Swain S, Rautray TR. Mechanism of ceramic coatings degradation. In: Gupta R, Motallebzadeh A, Kakooei S, Nguyen TA, Behera A, editors. *Advanced Ceramic Coatings for Biomedical Applications*. Vol. 23. 2023:33.
51. Dalby MJ, McCloy D, Robertson M, Wilkinson CD, Oreffo RO. Osteoprogenitor response to defined topographies with nanoscale depths. *Biomaterials*. 2006;27(8):1306–1315. doi:10.1016/j.biomaterials.2005.08.028
52. Türk S, İ A, Çelebi Efe G, Ipek M, Özacar M, Bindal C. Effect of solution and calcination time on sol-gel synthesis of hydroxyapatite. *J Bionic Eng*. 2019;16(2):311–318. doi:10.1007/s42235-019-0026-3
53. Venkatasubbu GD, Ramasamy S, Ramakrishnan V, Avadhani GS, Thangavel R, Kumar J. Investigations on zinc doped nanocrystalline hydroxyapatite. *Int J Nanosci Nanotechnol*. 2011;2(1):1–23.
54. James FZ, Ziegler MD, Biersack JP. SRIM – the stopping and range of ions in matter. *Nucl Instrum Methods Phys Res A*. 2010;268(11–12):1818–1823. doi:10.1016/j.nimb.2010.02.091
55. Rao KS, Anupama MP, Mahesh DG, Rao VR, Rautray TR, Venkateswarulu P. Trace elemental analysis of dental caries in human teeth by external PIXE. *Int J App Biol Pharm Technol*. 2010;1(1):68–78.
56. Huang Y, Zhang X, Zhang H, et al. Fabrication of silver-and strontium-doped hydroxyapatite/TiO2 nanotube bilayer coatings for enhancing bactericidal effect and osteoinductivity. *Ceram Int*. 2017;43(1):992–1007. doi:10.1016/j.ceramint.2016.10.031
57. Acciari HA, Palma DP, Codaro EN, et al. Surface modifications by both anodic oxidation and ion beam implantation on electropolished titanium substrates. *Appl Surf Sci*. 2019;487:1111–1120. doi:10.1016/j.apsusc.2019.05.216
58. Pecheva EV, Pramatarova LD, Maitz MF, Pham MT, Kondyuirin AV. Kinetics of hydroxyapatite deposition on solid substrates modified by sequential implantation of Ca and P ions: part I. *FTIR and Raman Spectroscopy Study Appl Surf Sci*. 2004;235(1–2):1.
59. Swain S, Rautray TR, Janssen D, Buma P, Grijpma DW. Silver doped hydroxyapatite coatings by sacrificial anode deposition under magnetic field. *J Mater Sci Mater Med*. 2017;28(1):1–5. doi:10.1007/s10856-016-5790-6
60. Narayanan R, Seshadri SK, Kwon TY, Kim KH. Calcium phosphate based coatings on titanium and its alloys: a review. *J Biomed Mat Res Part B*. 2008;85(1):279–299.
61. Rautray TR, Mohapatra B, Kim KH. Fabrication of strontium–hydroxyapatite scaffolds for biomedical applications. *Adv Sci Lett*. 2014;20(3):879–881. doi:10.1166/asl.2014.5424
62. Swain S, Bowen C, Rautray TR. Dual response of osteoblast activity and antibacterial properties of polarized strontium substituted hydroxyapatite—Barium strontium titanate composites with controlled strontium substitution. *J Biomed Mater Res Part A*. 2021;109(10):2027–2035. doi:10.1002/jbm.a.37195

63. Lu W, Zhou Y, Yang H, Cheng Z, He F. Efficacy of strontium supplementation on implant osseointegration under osteoporotic conditions: a systematic review. *J Prosthet Dent*. 2022;128(3):341–349. doi:10.1016/j.prosdent.2020.12.031
64. Agarwal A, Weis TL, Schurr MJ, et al. Surfaces modified with nanometer-thick silver-impregnated polymeric films that kill bacteria but support growth of mammalian cells. *Biomater*. 2010;31(4):680–690.
65. Morones JR, Elechiguerra JL, Camacho A, et al. The bactericidal effect of silver nanoparticles. *Nanotechnol*. 2005;16(10):2346. doi:10.1088/0957-4484/16/10/059
66. Cao H, Liu X, Meng F, Chu PK. Biological actions of silver nanoparticles embedded in titanium controlled by micro-galvanic effects. *Biomaterials*. 2011;32(3):693–705. doi:10.1016/j.biomaterials.2010.09.066
67. Khina AG, Krutyakov YA. Similarities and differences in the mechanism of antibacterial action of silver ions and nanoparticles. *Appl Biochem Microbiol*. 2021;57(6):683–693. doi:10.1134/S0003683821060053
68. Zhang E, Zou C. Porous titanium and silicon-substituted hydroxyapatite biomodification prepared by a biomimetic process: characterization and in vivo evaluation. *Acta Biomater*. 2009;5(5):1732–1741. doi:10.1016/j.actbio.2009.01.014
69. Cabrera WE, Schrooten I, De Broe ME, d'Haese PC. Strontium and bone. *J Bone Miner Res*. 1999;14(5):661–668. doi:10.1359/jbmr.1999.14.5.661
70. Lafzi A, Esmaeil Nejad A, Rezai Rad M, Namdari M, Sabetmoghaddam T. In vitro release of silver ions and expression of osteogenic genes by MC3T3-E1 cell line cultured on nano-hydroxyapatite and silver/strontium-coated titanium plates. *Odontology*. 2023;111(1):33–40. doi:10.1007/s10266-022-00747-z
71. Qiao H, Song G, Huang Y, et al. Si, Sr, Ag co-doped hydroxyapatite/TiO 2 coating: enhancement of its antibacterial activity and osteoinductivity. *RSC Adv*. 2019;9(24):13348–13364. doi:10.1039/C9RA01168D
72. Geng Z, Wang R, Zhuo X, et al. Incorporation of silver and strontium in hydroxyapatite coating on titanium surface for enhanced antibacterial and biological properties. *Mater Sci Eng C*. 2017;71:852–861. doi:10.1016/j.msec.2016.10.079
73. Li Y, Wang W, Han J, et al. Synthesis of silver- and strontium-substituted hydroxyapatite with combined osteogenic and antibacterial activities. *Biol Trace Elem Res*. 2022;200(2):931–942. doi:10.1007/s12011-021-02697-z